JOURNAL OF MECHANICAL ENGINEERING AND SCIENCES
ISSN: 2289-4659 e-ISSN: 2231-8380
VOLUME 18, ISSUE 4, 2024, 10279 - 10289
DOI: https://doi.org/10.15282/jmes.18.4.2024.5.0811

RESEARCH ARTICLE

Effect of internal partition on a naturally cross-ventilated generic building using computational fluid dynamics

Y. H. Fam[1], V. C. Tai[2], P. R. Mathew[1], Y. C. Tan[2], L. K. Moey[2]*

[1] Faculty of Engineering, Built Environment & Information Technology, SEGi University, 47810, Selangor, Malaysia

[2] Centre for Sustainable Design, Modelling and Simulation, Faculty of Engineering, Built Environment & Information Technology, SEGi University, 47810, Selangor, Malaysia

Phone:+60361451777; Fax.: 03-6145 1666

ABSTRACT – This research investigates natural ventilation characteristics for an isolated building, particularly air velocity and flow rate. It involves a numerical analysis using computational fluid dynamics for a generic building configuration with internal obstacles and under natural ventilation conditions. Internal obstacles within the building were modeled as internal partition walls with varying widths. Five different external opening configurations were considered: top-top, middle-middle, bottom-bottom, top-bottom and bottom-top. Atmospheric boundary layer conditions were imposed at the inlet plane. The 3-D Steady Reynolds Averaged Navier Stokes equations were solved with the Standard k-ε model and enhanced wall treatment. Results show that the highest dimensionless flow rate (DFR) is recorded at 0.568 for the top-top opening position without obstacle, while it is also observed that the varying internal obstacles have a substantial impact on the DFR. Hence, it could be concluded that ignoring the effects of partition walls or internal barriers in the study of natural ventilation can underestimate the DFR by as much as 11.2% as compared to an empty building setup. The study is able to provide useful information on the airflow characteristics for the natural ventilation application in the building sector.

ARTICLE HISTORY
Received : 25th June 2024
Revised : 22nd Sept. 2024
Accepted : 27th Nov. 2024
Published : 30th Dec. 2024

KEYWORDS
Computational fluid dynamics
Natural ventilation
Internal obstacles
Dimensionless flow rate

1. INTRODUCTION

Natural ventilation can provide the required air exchange in a building and remove undesired air pollutants from the interior when an effective design is adopted. The natural ventilation potential for a building evaluates the possibility of utilizing natural ventilation based on climatic conditions or specific building configurations [1]. The factors for driving natural ventilation are mainly wind movement and thermal buoyancy. Cross ventilation and single-sided ventilation are the types of wind-driven natural ventilation. Some previous studies, such as by Jiang et al. [2], generally concluded that single-sided ventilation is not as effective as cross-ventilation. Cross ventilation happens when there are two openings in a building and where such openings are opposite. The cross-ventilation performance can be affected by several factors, that include the opening shape [3], size [4,5], wind incidence angle [6] and the presence of louvers in a building [7,8]. Besides, the opening position within a building also plays an important factor and will affect the airflow pattern and the ventilation rate. Few studies from the literature concluded that the ventilation rate improves when the opening is closer to the top of the building [9,10]. Furthermore, opening closer to the bottom of the building at the windward side downplays the ventilation rate. Similarly, ventilation performance will also be affected when the opening is positioned at varying heights on the leeward and windward façade due to the varying pressure across the openings [11]. With the rapid advancement of technology in computing processes, computational fluid dynamics (CFD) is increasingly applied in natural ventilation studies as it can predict the airflow pattern, ventilation rate, and ventilation efficiency across all points within the computational domain with reasonable accuracy [12]. Besides, full-scale building models can be designed using CFD, unlike wind tunnel experiments using reduced-scale building models. The governing equation CFD uses is the Navier Stokes (N-S) equation. The N-S equations in turbulence modelling include Reynolds-Averaged Navier Stokes (RANS) and Large Eddy Simulation (LES). RANS turbulence model is frequently deployed as it has a reasonable balance between computational time and accuracy achieved [13].

Van Hooff et al. [14] executed a validation study through CFD based on the wind tunnel experimental results of Tominaga and Blocken [15]. RANS turbulence models were employed along with LES to study the effect of turbulence models on the parameters examined. The factor of two of observation analysis was deployed to determine the accuracy of the turbulence models in predicting the turbulent kinetic energy and dimensionless mean streamwise velocity across 7 vertical locations within the building. The Standard k-ε (SKE) performed better than the other RANS models. Nimarshana et al. [16] analyzed various turbulence models, and the results were comparatively assessed. The study showed that the SKE model performed better in replicating the airflow pattern inside the building. The influence of internal obstacles such as furniture or partition walls on ventilation rate prediction is limited within the natural ventilation studies. These obstructions to airflow act as internal resistance to the ventilation. Previous studies from the literature [17] investigated

*CORRESPONDING AUTHOR | L. K. Moey | ✉ moeylipkean@segi.edu.my

the influence of internal partition on buildings whereby the fan technique was used during the wind tunnel experiments. Several variables were studied, including the opening size and position within the partition plate. The findings suggest that the bigger opening size of the partition wall will result in a higher ventilation rate. Next, Chu and Chiang [18] conducted a wind tunnel study based on the influence of obstacle width, height and location within the reduced-scaled building. The internal obstacle was modelled as an internal partition wall. Increasing the partition width and height increased the internal blockage ratio, which reduced the dimensionless ventilation rate within the building. However, the drawback of this study was that only one opening position was considered. To the authors' knowledge, no studies from the literature analysed the opening position of a building and the presence of internal obstacles. Therefore, this study aims to investigate the effect of opening positions with the presence of internal obstacles on the dimensionless flow rate. This paper is organized as follows: section 2 stipulates the methodology used for this study, section 3 shows the results and the discussion, and lastly, section 4 presents the study's conclusion.

2. MATERIALS AND METHODS

2.1 Building Model Geometry

The building model adopted in this present study was based on the generic building by van Hooff et al. [14]. This model was used in the wind tunnel study by Tominaga and Blocken [15], two years prior to the CFD study done by van Hooff et al. [14]. This building model used is a reduced scaled model of 1:100. The building dimension in reduced scale is 0.2 m × 0.2 m × 0.16 m ($L \times W \times H$), and CFD simulation was conducted on this reduced scale model for result comparison and verification purpose. The model is equipped with two openings aligned in the center plane and opposite each other, and the window opening dimension is 0.092 m × 0.036 m ($L \times H$). The orientation of the opening position is perpendicular to the direction of the incoming wind, and the wall thickness of the model, ζ is uniform across all surfaces at 3 mm. Thus, this building model has a wall porosity of 10.35%.

Table 1. Simulation cases

Case	Parameter Studied	Manipulated Variable	Opening Position	Batch
1	Empty building	Opening position	Top-Top	1
2			Middle-Middle	
3			Bottom-Bottom	
4			Top-Bottom	
5			Bottom-Top	
6	Width of partition (20% W)	Opening position and the width of a partition wall	Top-Top	2
7			Middle-Middle	
8			Bottom-Bottom	
9			Top-Bottom	
10			Bottom-Top	
11	Width of partition (40% W)		Top-Top	
12			Middle-Middle	
13			Bottom-Bottom	
14			Top-Bottom	
15			Bottom-Top	
16	Width of partition (60% W)		Top-Top	
17			Middle-Middle	
18			Bottom-Bottom	
19			Top-Bottom	
20			Bottom-Top	
21	Width of partition (80% W)		Top-Top	
22			Middle-Middle	
23			Bottom-Bottom	
24			Top-Bottom	
25			Bottom-Top	

Twenty-five simulation cases were conducted in this study. Five varying opening positions were simulated and assessed against four configurations of internal partition walls to model the effect of internal blockage. The five opening positions considered in this research were Top-Top, Middle-Middle, Bottom-Bottom, Top-Bottom and Bottom-Top. Batch 1 of the study considers the opening position with an empty building (i.e. no internal partition), while Batch 2

consists of 20 cases with four varying internal partition widths. The summary of the simulation cases carried out is tabulated in Table 1.

2.1.1 Batch 1 - Empty building

Batch 1 of this study focuses on varying opening positions on an empty building, whereby the opening positions were located in the center plane of the building. Five simulation cases were classified within this batch. Figure 1(a)-(c) shows the side view for the various opening positions. The center of the opening for the top, middle, and bottom is 40 mm, 80 mm and 120 mm above the ground surface, as indicated in Figure 2. To simulate a symmetry condition, the building was cut in half symmetrically, as shown in the isometric view in Figure 1(d). This is to reduce the computational time for the simulation.

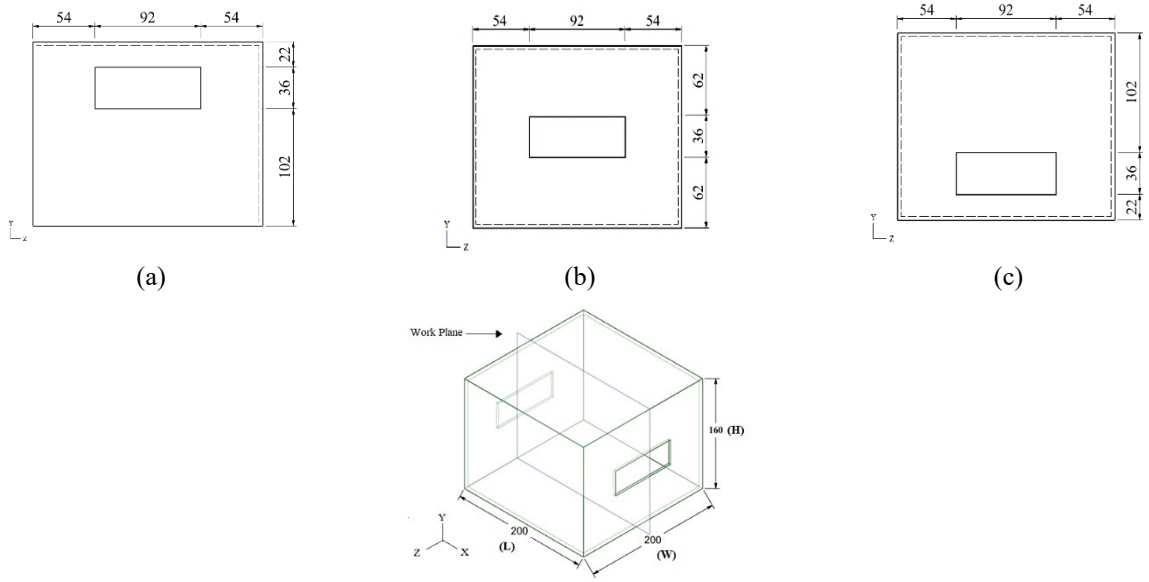

(a) (b) (c)

(d)

Figure 1. Building configurations with opening position at: (a) Top-Top, (b) Middle-Middle, (c) Bottom-Bottom and (d) Work plane

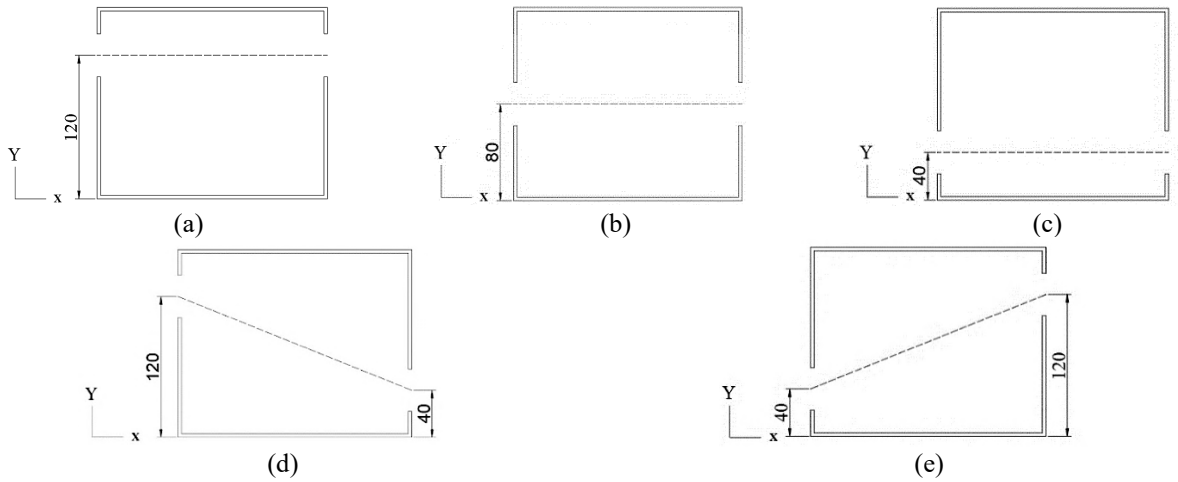

(a) (b) (c)

(d) (e)

Figure 2. Opening locations from ground surface: (a) Top-Top, (b) Middle-Middle, (c) Bottom-Bottom, (d) Top-Bottom and (e) Bottom-Top

2.1.2 Batch 2 – With the influence of the internal partition wall

In this series, the width of the partition wall varied along with the opening position, while other parameters such as the wall thickness, the partition wall's height, the partition wall, and the location of the partition wall from the windward opening were the same. The thickness of the partition wall is the same as the wall thickness of the building, which is 3 mm, while the height of the partition wall is 120 mm or 75% of the building height. To manipulate the partition width, the internal blockage ratio (r_p), the formula shown in Eq. (1) is used to quantify the partition width area to the building interior area as used by Chu and Chiang [18]. The area of the building cross section, A_i is 0.032 m^2. Meanwhile, the partition's width was adjusted to 40 mm, 80 mm, 120 mm and 160 mm. Since the building width is 200 mm, the width

of the partition wall is in the range of 20%, 40%, 60% and 80% of the building width, respectively (see Figure 3). Consequently, this resulted in a blockage ratio of 0.15, 0.3, 0.45 and 0.6 as shown in Table 2.

$$r_p = \frac{A_p}{A_i} \tag{1}$$

where, r_p is the internal blockage ratio, A_p is the area of internal partition wall (W×H) in m^2, A_i is the area of building interior (W×H) in m^2.

Table 2. Internal blockage ratio for Batch 2 simulation cases

Partition Wall Parameter	W×H (m^2)	A_p (m^2)	A_i (m^2)	r_p
No blockage	-	-		0
20% width, 20% W	0.04×0.12	0.0048		0.15
40% width, 40% W	0.08×0.12	0.0096	0.032	0.30
60% width, 60% W	0.12×0.12	0.0144		0.45
80% width, 80% W	0.16×0.12	0.0192		0.60

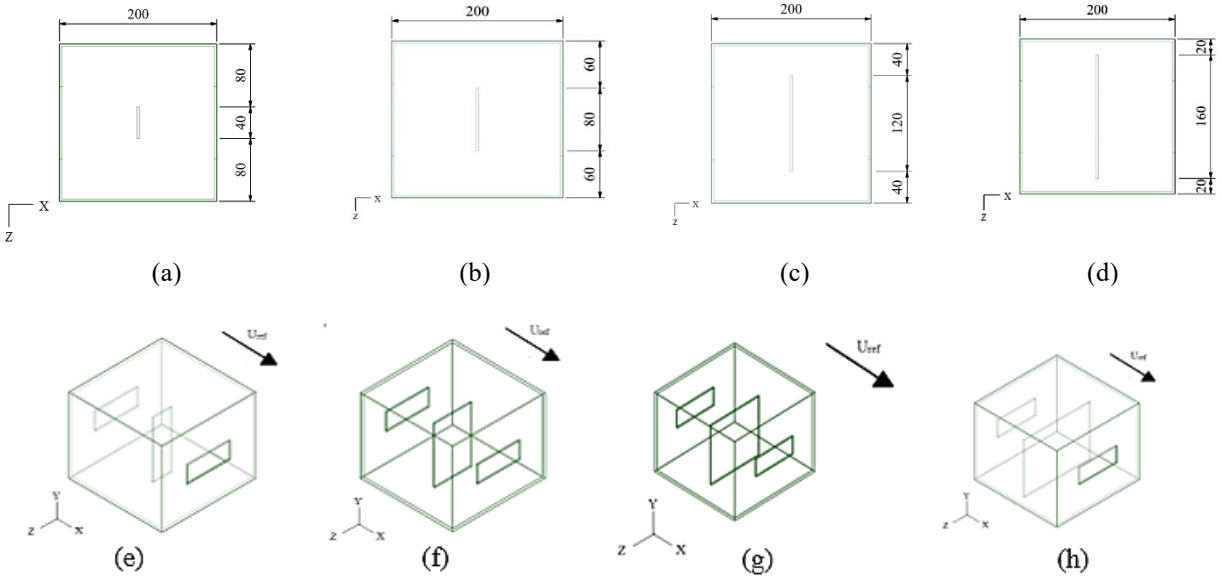

Figure 3. Top view of Batch 2 cases at: (a) 20% W, (b) 40% W, (c) 60% W, (d) 80% W, and isometric view at (e) 20% W, (f) 40% W, (g) 60% W and (h) 80% W

2.2 Computational Domain

The computational domain was generated based on the model geometry outlined in section 2.1 above. The body of influence (BOI) for the entire building was first created. Then, the BOI for the windward and leeward opening positions were designed. Figure 4(a) illustrates the isometric view of the flow domain, while Figures 4(b) and 4(c) show the front view and the side view of the domain, respectively. The flow domain shown in Figure 4(a)(vi) and 4(a)(i) are the Leeward BOI, while 4(a)(ii) shows the Windward BOI, 4(a)(iii) is the building BOI, 4(a)(iv) is the near BOI and finally 4(a)(v) is the far BOI.

The flow domain was designed such that the building model to the sides of the flow domain has a distance of 5H (building height, H at 160 mm), while the leeward side of the building model to the outlet plane of the flow domain has a distance of 15H. This is to ensure that the flow is substantially developed. On the other hand, to avoid unintended streamwise gradients in the approach-flow profile, the inlet plane was fixed at 3H from the windward side of the building [12,19]. Furthermore, the blockage ratio of the building area to the frontal area of this domain is 1.85%, less than 3%. The flow domain was designed to comply with CFD guidelines [20, 21, 22].

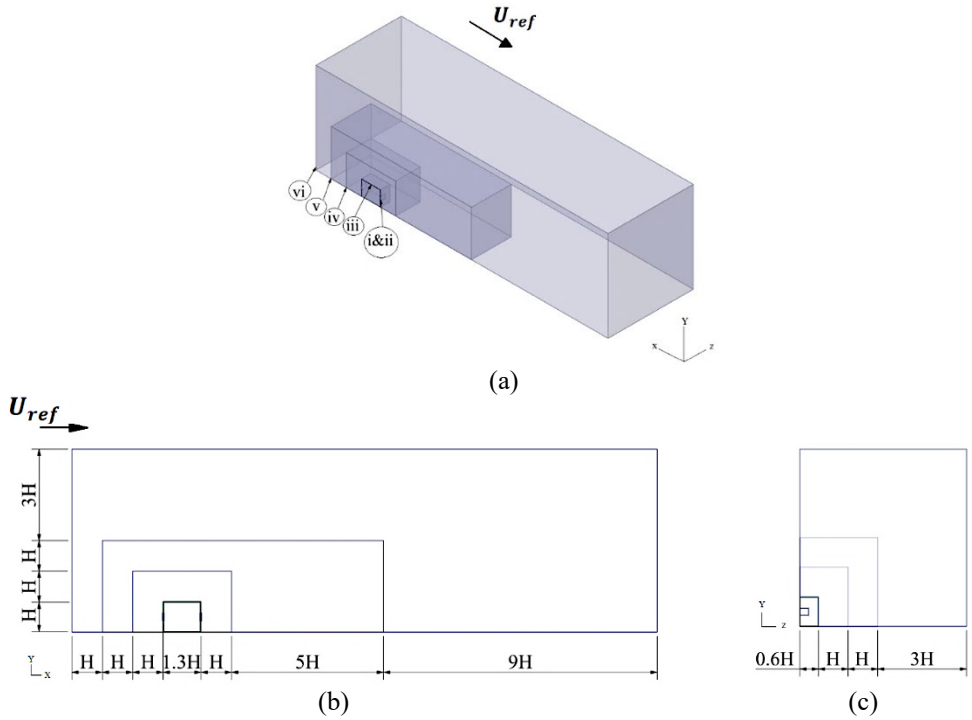

Figure 4. Computational domain in the (a) Isometric view, (b) Front view and (c) Side view

2.3 Mesh Generation

This study generated the volume mesh using ANSYS 2020 R1 Fluent with Fluent Meshing. The Watertight Geometry Workflow task was selected, and the geometry file with the named selections was imported into the software. Subsequently, the local scope sizing was imposed on several sections within the flow domain. A domain called the BOI surrounded the geometry of the building within the flow domain [23, 24]. Firstly, a BOI was constructed to encompass the building itself, which is finer than the other scope sizing applied. Next, a separate BOI surrounded the windward and leeward openings. These BOIs aimed to capture the airflow through the openings. The fourth BOI, near BOI, was created to refine the mesh closer to the building itself. Lastly, the fifth BOI, the far BOI, was made to capture the approaching flow and the flow separation effects at the leading edge. Since the building is considered a bluff body with sharp edges, flow separation at the roof of the house is bound to occur, especially with a high Reynolds number of 47,000, which indicates a turbulent flow. Curvature sizing was also imposed on the building to refine the mesh around the edges of the house. The global scope sizing was imposed onto the surface mesh upon the completion of the local sizing. The growth rate of the surface mesh was kept to 1.05 for a smooth transition from the flow domain approaching the house, while the local scope sizing growth rate was constant at 1.2, which is within the allowable grid stretching ratio [20].

The volume mesh was created once the surface mesh had been generated, as seen in Figure 5. Poly-hexcore volume mesh was selected along with 15 last ratio prism layers surrounding the building and the partition wall, as seen in Figure 5. Zore et al. [25] infer that the advantage of using Poly-hexcore mesh is that the simulation time is reduced by 10-50% and cell count reduction by 20-50%. The first cell height used is 35μm based on the y+ value of 1 to resolve the flow down to the wall, concurrently resolving the viscous sublayer since the y+ within this turbulent boundary layer is less than 5. A normal curvature angle of 10° with 2 cells per gap was set as well. Lastly, the target cell quality limit is set at 0.35, resulting in an inverse orthogonal quality of 0.65, which is also considered acceptable.

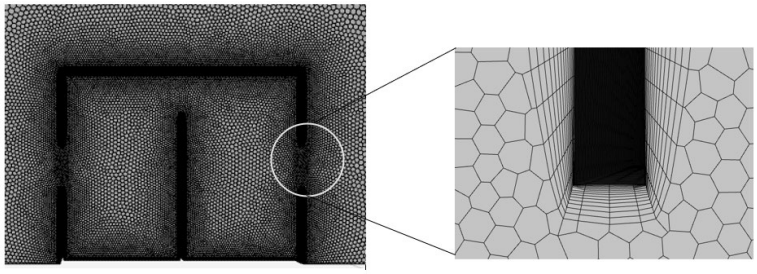

Figure 5. Poly-hexcore mesh surrounding the partition wall within the house

2.4 Atmospheric Boundary Layer

The atmospheric boundary layer (ABL) was imposed during the wind tunnel test of the reference case. The ABL equations were realized through a user-defined function (UDF), a C++ format file to be compiled into ANSYS Fluent, as

these equations are not defined within the Fluent solver. The aerodynamic roughness length, z_o used was 0.0009 *m,* and z is the height coordinate. The ABL friction velocity, u^*_{ABL} used was 0.348 m/s, while Von Karmann's constant, κ was at 0.42. Hence, the resulting mean streamwise velocity is shown in Eq. (2).

$$U(z) = \frac{u^*_{ABL}}{\kappa} ln \left(\frac{z + z_o}{z_o}\right) \tag{2}$$

Next, the turbulent kinetic energy, k profile was obtained by measuring the variance in the mean streamwise velocity fluctuations in the x, y and z directions. The reference velocity at building height (U_H) was 4.3 m/s. The resulting equation can be approximated by Eq. (3). Subsequently, the turbulent dissipation rate ε was calculated using Eq. (4) [26]. The specific turbulent dissipation rate, ω in Eq. (5) was calculated as well from the turbulent dissipation rate, ε with the relation of the k profile and C_μ which has a constant value of 0.09.

$$\left(\frac{k(z)}{U_H^2}\right) = 0.033e^{-0.32\left(\frac{z}{H}\right)} \tag{3}$$

$$\varepsilon = \frac{(u^*_{ABL})^3}{\kappa(z + z_o)} \tag{4}$$

$$\omega = \frac{\varepsilon}{C_\mu k} \tag{5}$$

Besides, certain boundary conditions were imposed within the flow domain. The inlet plane was defined as the velocity inlet whereby the velocity magnitude and turbulence along with the k, ε and ω profiles were defined by the UDF profiles in the Fluent solver. Next, the outlet plane of the flow domain was set as the pressure outlet, whereby all the normal gradients of all variables are zero to ensure a fully developed flow [20]. Other than that, the top and side walls of the domain were set to symmetry conditions as it is usually prescribed to do so to enforce a parallel flow [22].

2.5 Grid Sensitivity Analysis

Grid sensitivity analysis was conducted for the middle-middle opening position case using the SKE turbulence model coupled with the EWT. Three different grids were generated to assess the degree of error to the point where it would reach an asymptotic value. The coarse, medium, and fine grids have a cell count of 2,466,031, 2,897,126, and 3,818,786, respectively. Next, the grid convergence index (GCI) [27] was applied to estimate the error of the dimensionless mean streamwise velocity (U/U_{ref}) from the coarse grid and medium grid against the fine grid. The GCI equation is shown in Eq. (6), where the safety factor (SF) is considered 1.25 when 3 or more grids are considered. Next, the grid refinement factor, r used was $\sqrt{2}$ and the formal order of accuracy, p was 2 since second-order discretization schemes were used. Three vertical lines were established within the building at locations of x/D = 0.125, x/D = 0.5, and x/D = 0.875, and the average of the GCI results were taken, as tabulated in Table 3. The parameter 'D' is the building length, while the parameter 'x' is the varying length referenced within the building. For the coarse grid, the average GCI along the vertical lines of x/D = 0.125, x/D = 0.5, and x/D = 0.875 are 1.01%, 2.16% and 1.09%, respectively. On the other hand, the medium grid gives an average GCI of 0.67%, 1.4% and 0.8% along the vertical lines of x/D = 0.125, x/D = 0.5, x/D = 0.875, respectively. In conjunction with that, it can be observed that the average GCI reduces when comparing the medium grid and the fine grid across all vertical line measurements used. Based on the results, the average GCI for the coarse grid is 1.42%, while for the medium grid is 0.96%. Thus, the medium grid is adopted for the remainder of the simulations since it has a lower GCI obtained, which is less than 1% and desirable.

$$GCI = SF \left| \frac{r^p \frac{U_{coarse} - U_{fine}}{U_{ref}}}{r^p - 1} \right| \tag{6}$$

Table 3. GCI values across three vertical lines were measured

Location	Grid Convergence Index (GCI)	
	Coarse vs. Fine	Medium vs. Fine
x/D = 0.125	1.01	0.67
x/D = 0.5	2.16	1.40
x/D = 0.875	1.09	0.80
Average	1.42	0.96

3. RESULTS AND DISCUSSION

3.1 Dimensionless Mean Streamwise Velocity U/U_{ref}

The velocity recorded in the building is dimensionless by dividing the velocity magnitude by the reference velocity at building height, U_{ref} of 4.3 m/s. The resulting dimensionless mean streamwise velocity contours are shown in Table 4 for Batches 1 and 2 of the simulation cases. Simulation Batch 1 considered the opening position on a building without any partition wall (NP) as a comparison for a building with internal partitions regarding the airflow pattern obtained. Batch 2 considered the impact of increasing partition width on the internal airflow pattern within the building while keeping the partition height and location from the windward wall constant at x/D = 0.5.

Regarding the empty building, a significantly large area across all opening positions is observed to have a low-magnitude velocity gradient, either above or below the incoming jet. When a partition wall was added, the location of this low-velocity gradient was observed to have shifted. Across all opening configurations, it is generally noted that a low-velocity gradient or recirculation zone was formed upstream and downstream of the partition wall regardless of the partition width (blockage ratio). For instance, at the top-top opening position, the stagnation region upstream of the partition wall reduced magnitude when the partition width increased from 20% to 40%. The same trend could be seen downstream of the partition wall, where the low-velocity regions decrease in magnitude, especially when the wall width is increased from 40% to 80%. Another interesting observation is the deflection of the incoming streamwise velocity jet as it hit the partition wall, which could be seen for the top-top configuration paired with the 80% partition wall width. Besides, for the top-bottom opening configuration, increasing the partition width to 60% and 80% of the building width results in a greater dissipation of the incoming jet as it hits the partition wall. This is because the partition wall height coincides with the center of the opening at the top-top position. Based on the contours, it could be deduced that the top-top and top-bottom configurations experienced a difference in the stagnation region in front and behind the partition wall. This is because the top-bottom configuration has a smaller stagnation zone surrounding the partition wall when the partition width or blockage ratio increases. In addition, the outgoing velocity jet for the top-bottom opening position could be seen to be angled upwards and remains horizontal from the no-partition configuration up to the 80% W configuration.

The inlet jet is more horizontal for the middle-middle opening configuration than the empty building case since the air is directed to the partition wall at the center of the building. Then, it could also be seen that there is a stagnation zone at the ceiling, which is reduced when a partition wall is added to this opening configuration. The stagnation region at the ceiling shifts further downstream of the partition wall as the width increases from 40% to 60% until there is essentially little to none of this stagnation zone at the ceiling. Instead, this stagnation or low-velocity magnitude zone builds downstream of the partition wall, which could be observed from 40% W up to 80% W partition setup. The outlet jet is also seen to be altered from being angled upwards to being more horizontal as the blockage ratio increases. Similarly, the magnitude of the outlet jet also reduces. The Coanda effect could be seen for the bottom-bottom opening position without any obstacles as the incoming jet is directed downwards into the enclosure, which is attributed to the standing vortex in front of the building, as mentioned by Tominaga and Blocken [11]. However, the flow pattern changes when a partition wall is added, whereby the incoming jet is impinged on the wall and directed upwards instead of following the ground surface path. Similar to the middle-middle opening position, a stagnation zone at the ceiling is also observed. Increasing the partition width shifts the stagnation zone downstream of the partition wall and reduces the low-magnitude velocity zone. The outlet jet is angled upwards at first and subsequently transitioned to flow horizontally and finally angled downwards at 80% W partition setup. It is also observed that the outlet jet reduces in magnitude with increased partition width. This is because of the increase in the blockage ratio when the partition width increases. Generally, the bottom-top opening configuration shows a similar flow pattern to the bottom-bottom configuration. However, instead of having the stagnation region focus on the upper part of the enclosure, the stagnation zone of the bottom-top configuration focuses downstream of the partition wall as the width of the wall increases, especially from 60% to 80%W partition design. The outlet jet for this configuration is also observed to angle horizontally when a partition wall is added.

According to the U/U_{ref} contours of the increasing partition width, a general summary can be made to explain the phenomenon of the shifting of the stagnation zone across all opening positions. Considering the middle-middle, bottom-bottom and bottom-top opening positions, the partition wall height adopted in these configurations covers the opening as the partition wall height covers 75% of the building height. When a partition wall is placed starting from the minimum width, the airflow could still pass through the sides of the wall as there was a gap between the partition wall and the building wall. As the partition width further increases up to 80% W, it results in a scenario where the airflow is forced to pass through the top of the partition wall instead of the space between the building wall and the partition wall due to the increased blockage. Contrary to this, increasing the partition width for the top-top opening setup causes a portion of the incoming jet to deflect and reduce in magnitude upon hitting the wall, which in turn reduces the stagnation zone in front of the partition wall while reducing the stagnation zone magnitude slightly downstream of the partition wall. The top-bottom configuration also encounters a similar flow pattern. Still, a better reduction in the stagnation zone is observed since the outlet was at the bottom, which forces the approaching flow of air to be directed downwards.

3.2 Dimensionless k/U_{ref}^2

The effect of the turbulent kinetic energy, k is also recorded in the present simulation. It is made to be dimensionless by dividing k over the reference velocity at the building height squared. The contours of the turbulent kinetic energy are

shown in Table 5. A general observation is that the spreading of the incoming jet occurred as it impinges onto the partition wall in all partition width across all opening positions. For instance, the middle-middle configuration shows the jet impinged further up to the ceiling when the partition width is increased to 40% W and deflects further downstream of the wall with an increase in partition width. The same is noticed for the bottom-top and bottom-bottom opening positions. Besides, the top-top and top-bottom configurations also show a similar relationship based on the contours observed where the jet initially deflects downwards after impinging on the partition wall but travels in a straight and horizontal direction as the partition width increases.

3.3 Dimensionless Flow Rate

After examining the dimensionless streamwise velocity contours, the volume flow rate through the building can be calculated to determine the effect of the partition wall on the ventilation rate. Using the Fluent CFD software, a plane was created in the windward opening position, whereby the volume flow rate can be calculated. Then, it is made dimensionless by dividing the volume flow rate over the product of the reference velocity of 4.3 m/s along with the opening area of 0.0033 m^2. The effect of internal obstacles such as an office partition, furniture or even the occupants within the building were not considered in previous studies, and the ventilation rate tends to be overestimated or underestimated due to the added blockage to internal airflow was not accounted for. Hence, the dimensionless flow rate (DFR) is used to quantify the impacts of the increased blockage ratio on the DFR obtained.

Firstly, the influence of increasing internal partition width on the dimensionless flow rate is determined. The DFR for all partition configurations, i.e. NP, 20% W, 40% W, 60% W and 80% W are shown in Figure 6. The NP or no partition wall configuration with the top-top opening position results in the highest recorded DFR, followed by the top-bottom, middle-middle and bottom-bottom opening positions, while the bottom-top recorded the lowest. The DFR of the NP configuration from highest to lowest are 0.568, 0.486, 0.483, 0.456 and 0.405. These findings are consistent with the existing literature, whereby the top-top opening position results in a better ventilation rate in a building [9–11,24]. Similarly, Tominaga and Blocken [11] inferred that the influence of the inlet opening position affects the pressure difference, facilitating cross ventilation. When the partition wall is added, it could be observed that a decreasing trend of DFR values was recorded for the symmetrically aligned opening positions. This observation is visible for the middle-middle and bottom-bottom opening positions. Furthermore, the bottom-bottom opening position records a substantial drop in DFR of up to 9% from 0.456 to 0.416 when a partition wall is introduced into the building (20% W configuration). Increasing the partition width up to 80% W does not lead to any significant drop in DFR. In addition, the DFR for the middle-middle opening configuration decreases by 3.1% when a partition wall is added at 20% W. Increasing the partition width decreases the DFR gradually from 0.468 to 0.454 at 80% W configuration. These results are similar to the results obtained by Chu and Chiang [18], where an increased blockage ratio with increasing partition width reduces the dimensionless ventilation rate. However, the study by Chu and Chiang did not consider the impacts of varying opening positions along with the partition wall width.

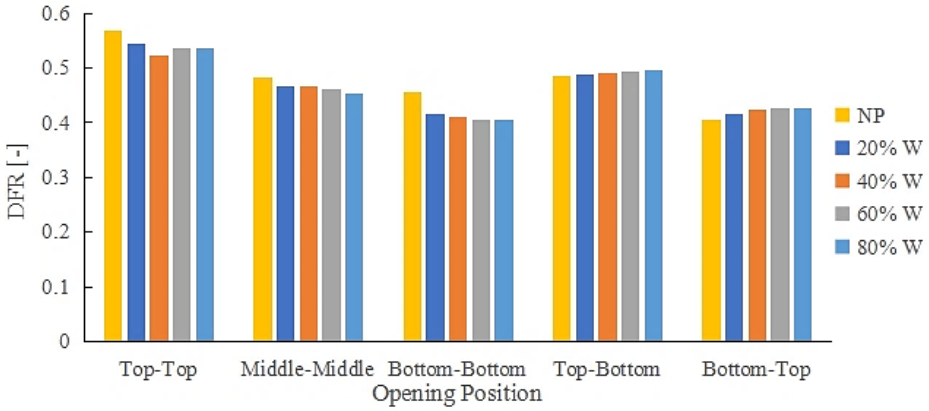

Figure 6. Dimensionless flow rate for Batch 1 and 2 simulations

Meanwhile, the top-top opening position shows a decreasing trend from NP configuration up to 40% W, with a reduction of 8% in DFR recorded from 0.568 to 0.523. However, the DFR increases gradually from 0.523 to 0.537 at 80% partition width. Overall, the DFR records for increasing partition width for the top-top opening position is less than the NP configuration due to the increased internal blockage ratio. Interestingly, the top-bottom and bottom-top opening positions record an increase in DFR when the partition width increases. This contradicts the expectation that increasing the partition width will reduce the DFR regardless of the opening position. The bottom-top configuration with 60% W and 80% W show an increase of 5.2% in the DFR obtained. Similarly, the increase in DFR for the bottom-top opening position is even clearer compared to the top-bottom position. This can be attributed to the reduction of the stagnation zone at the ceiling and downstream of the partition wall with the increase in partition width. Conversely, the bottom-bottom configuration experiences a greater drop in DFR relative to the bottom-top opening position. The result shows that the influence of the outlet opening at different heights does play a role in improving the DFR for a partitioned and non-partitioned building.

Table 4. U/U_{ref} contours for batch 1 and 2 simulations

Config.	Legend	No partition	20% W	40% W	60% W	80% W
Top-Top	U/U_{ref} [-] 1.35 1.25 1.16 1.06 0.96 0.86 0.77 0.67 0.57 0.47 0.38 0.28 0.18 0.08 -0.01 -0.11 -0.21 -0.31 -0.40 -0.50	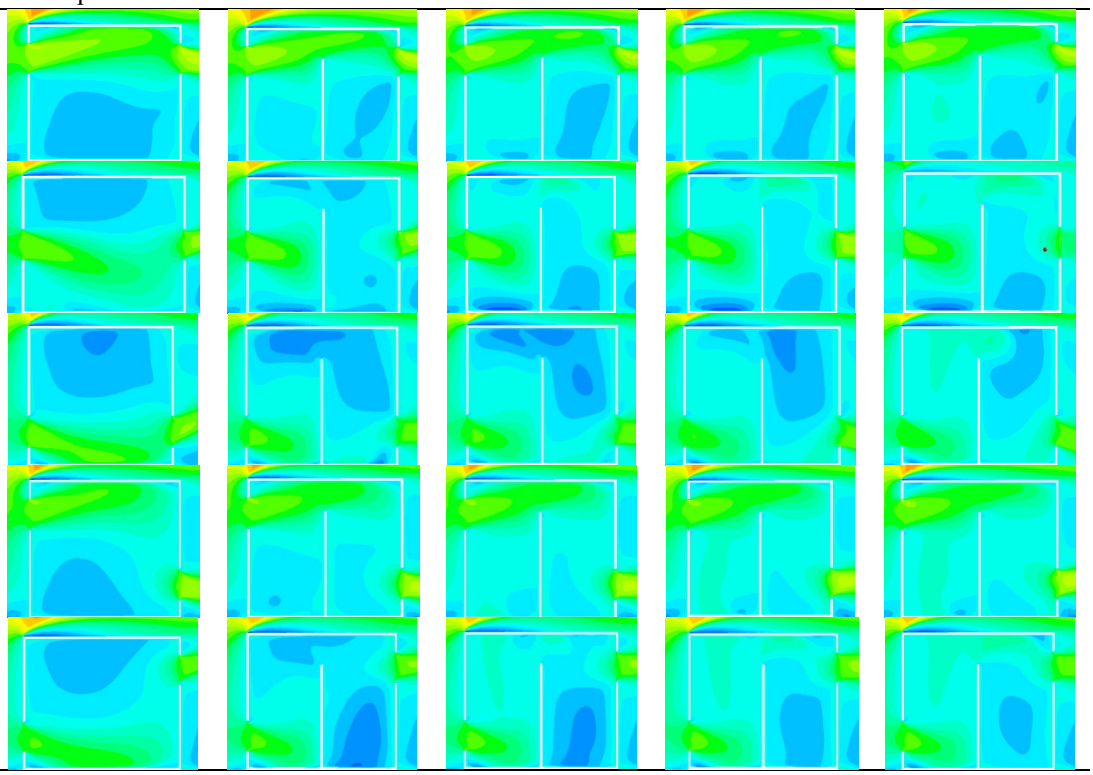				
Middle-Middle						
Bottom-Bottom						
Top-Bottom						
Bottom-Top						

Table 5. Dimensionless $(k/U_{ref}{}^2)$ contours for batch 1 and 2 simulations

Config.	Legend	No partition	20% W	40% W	60% W	80% W
Top-Top	$k/U_{ref}{}^2$ [-] 0.22 0.21 0.20 0.18 0.17 0.16 0.15 0.14 0.13 0.11 0.10 0.09 0.08 0.07 0.06 0.05 0.03 0.02 0.01 0.00	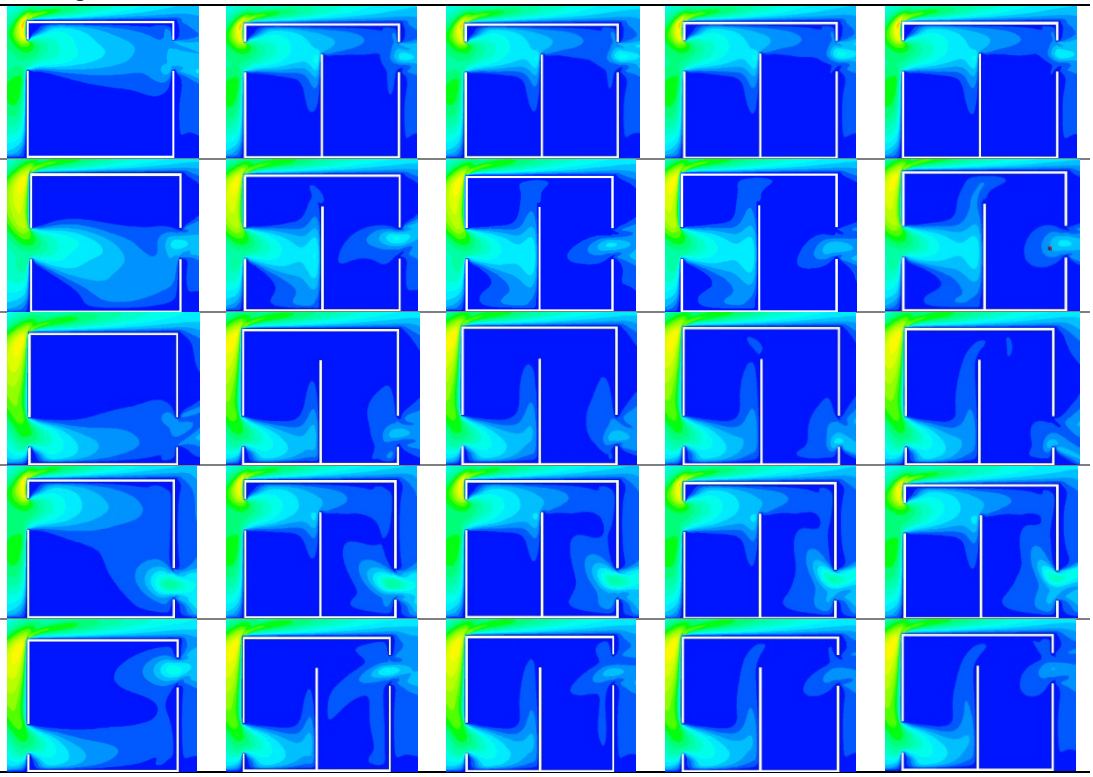				
Middle-Middle						
Bottom-Bottom						
Top-Bottom						
Bottom-Top						

4. CONCLUSIONS

The influence of the opening positions, together with the presence of varying internal obstacles, have been analyzed in the study. The opening positions considered were the top-top, middle-middle, bottom-bottom, top-bottom and bottom-top, whereas the configurations adopted in the study were windward-leeward. A partition wall of varying widths represented the obstacle within the building. GCI analysis was also conducted, and the medium grid was selected as it

obtained a GCI value of less than 1%. The findings from the study indicate that openings closer to the top of the building generate higher DFR regardless of the partition wall configuration used. The highest DFR obtained in the simulations is 0.568 for the top-top opening position without obstacles. The results are coherent with the findings from existing literature. The study also reveals that increasing the partition width reduces the DFR as the symmetrical openings move closer to the bottom of the building. Besides, the DFR could be increased by placing the partition wall in a building for bottom-top and top-bottom configurations. Finally, comparing the outcomes of the 25 simulation cases conducted in this study, it could be deduced that by ignoring the effect of internal partition walls or internal obstacles in a building, the airflow velocity and flow profiles could be substantially different and overestimated. In the case of a building with an internal partition of 80% of the building width in the study, it brings about a drop of 11.2% in the calculated DFR in the bottom-bottom opening position. The study was conducted in an isolated building setting. It is suggested that similar research be conducted on buildings in urban settings where other buildings surround the target building.

ACKNOWLEDGEMENTS

The project is funded by SEGi University under the SEGi Internal Research Fund. Grant No: SEGiIRF/2023-Q1/FoEBEIT/031.

CONFLICT OF INTEREST

The authors declare no conflicts of interest.

AUTHORS CONTRIBUTION

Y. H. Fam (Writing – original draft; Visualization; Investigation; Formal analysis; Data curation)

V. C. Tai (Writing – review & editing; Software; Conceptualization)

P. R. Mathew (Writing – original draft; Validation; Methodology; Formal analysis)

Y. C. Tan (Supervision; Validation; Resources)

L. K. Moey (Supervision; Project administration; Funding acquisition; Conceptualization)

AVAILABILITY OF DATA AND MATERIALS

The data supporting this study's findings are available on request from the corresponding author.

ETHICS STATEMENT

Not applicable.

REFERENCES

[1] N. R. M. Sakiyama, L. Mazzaferro, J. C. Carlo, T. Bejat, H. Garrecht, "Natural ventilation potential from weather analyses and building simulation," *Energy and Buildings*, vol. 231, p. 110596, 2021.

[2] Y. Jiang, D. Alexander, H. Jenkins, R. Arthur, Q. Chen, "Natural ventilation in buildings: Measurement in a wind tunnel and numerical simulation with Large-Eddy simulation," *Journal of Wind Engineering and Industrial Aerodynamics*, vol. 91, no. 3, pp. 331–353, 2003.

[3] H. Shetabivash, "Investigation of opening position and shape on the natural cross ventilation," *Energy Building*, vol. 93, pp. 1–15, 2015.

[4] L. K. Moey, Y. H. Sing, V. C. Tai, T. F. Go, Y. Y. Sia, "Effect of opening size on wind-driven cross ventilation," *International Journal of Integrated Engineering*, vol. 13, no. 6, pp. 99–108, 2021.

[5] H. Sacht, M. A. Lukiantchuki, "Windows size and the performance of natural ventilation," *Procedia Engineering*, vol. 196, pp. 972–979, 2017.

[6] T. S. Larsen, P. Heiselberg, "Single-sided natural ventilation driven by wind pressure and temperature difference," *Energy and Buildings*, vol. 40, no. 6, pp. 1031–1040, 2008.

[7] K. Kosutova, T. Van Hooff, B. Blocken, J. Hensen, "CFD analysis of ventilative cooling in a generic isolated building equipped with ventilation louvers," in *Healthy Buildings Europe*, Eindhoven, Netherlands, 2015.

[8] K. Kosutova, T. Van Hooff, C. Vanderwel, B. Blocken, J. Hensen, "Cross-ventilation in a generic isolated building equipped with louvers: Wind-tunnel experiments and CFD simulations," *Building and Environment*, vol. 154, pp. 263–280, 2019.

[9] P. Karava, T. Stathopoulos, A. K. Athienitis, "Airflow assessment in cross-ventilated buildings with operable façade elements," *Building and Environment*, vol. 46, no. 1, pp. 266–279, 2011.

[10] N. F. M. Kasim, S. A. Zaki, M. S. M. Ali, N. Ikegaya, A. A. Razak, "Computational study on the influence of different opening position on wind-induced natural ventilation in urban building of cubical array," *Procedia Engineering*, vol. 169, pp. 256–263, 2016.

[11] Y. Tominaga, B. Blocken, "Wind tunnel analysis of flow and dispersion in cross-ventilated isolated buildings: Impact of opening positions," *Journal of Wind Engineering and Industrial Aerodynamics*, vol. 155, pp. 74–88, 2016.

[12] R. Ramponi, B. Blocken, "CFD simulation of cross-ventilation for a generic isolated building: Impact of computational parameters," *Building and Environ*ment, vol. 53, pp. 34–48, 2012.

[13] B. Blocken, "50 years of computational wind engineering: Past, present and future," *Journal of Wind Engineering and Industrial Aerodynamics*, vol. 129, pp. 69–102, 2014.

[14] T. Van Hooff, B. Blocken, Y. Tominaga, "On the accuracy of CFD simulations of cross-ventilation flows for a generic isolated building: Comparison of RANS, LES and experiments," *Building and Environment*, vol. 114, pp. 148–165, 2017.

[15] Y. Tominaga, B. Blocken, "Wind tunnel experiments on cross-ventilation flow of a generic building with contaminant dispersion in unsheltered and sheltered conditions," *Building and Environment*, vol. 92, pp. 452–461, 2015.

[16] P. H. Nimarshana, R. A. Attalage, K. K. C. Perera, "Quantification of the impact of RANS turbulence models on airflow distribution in horizontal planes of a generic building under cross-ventilation for prediction of indoor thermal comfort," *Journal of Building Engineering*, vol. 52, p. 104409, 2022.

[17] C. R. Chu, Y. H. Chiu, Y. W. Wang, "An experimental study of wind-driven cross ventilation in partitioned buildings," *Energy and Buildings*, vol. 42, no. 5, pp. 667–673, 2010.

[18] C. R. Chu, B. F. Chiang, "Wind-driven cross ventilation with internal obstacles," *Energy and Buildings*, vol. 67, pp. 201–209, 2013.

[19] B. Blocken, T. Stathopoulos, J. Carmeliet, "CFD simulation of the atmospheric boundary layer: Wall function problems," *Atmospheric Environment*, vol. 41, no. 2, pp. 238–252, 2007.

[20] Y. Tominaga, A. Mochida, R. Yoshie, H. Kataoka, T. Nozu, M. Yoshikawa, et al., "AIJ guidelines for practical applications of CFD to pedestrian wind environment around buildings," *Journal of Wind Engineering and Industrial Aerodynamics*, vol. 96, no. 10–11, pp. 1749–1761, 2008.

[21] B. Blocken, "Computational fluid dynamics for urban physics: Importance, scales, possibilities, limitations and ten tips and tricks towards accurate and reliable simulations," *Building and Environment*, vol. 91, pp. 219–245, 2015.

[22] J. Franke, C. Hirsch, G. Jensen, H. W. Krus, S. D. Miles, M. Schatzmann, et al., "Recommendations on the use of CFD in wind engineering," in *COST Action C14, Impact of Wind and Storm on City Life and Built Environment*, 2004.

[23] T. Van Hooff, B. Blocken, "Coupled urban wind flow and indoor natural ventilation modelling on a high-resolution grid: A case study for the Amsterdam Arena stadium," *Environmental Modelling Software*, vol. 25, no. 1, pp. 51–65, 2010.

[24] L. K. Moey, K. L. Chan, V. C. Tai, T. F. Go, P. L. Chong, "Investigation on the effect of opening position across an isolated building for wind-driven cross ventilation," *Journal of Mechanical Engineering and Sciences,* vol. 15, no. 2, pp. 8141–8152, 2021.

[25] K. Zore, B. Sasanapuri, G. Parkhi, A. Varghese, "ANSYS mosaic poly-hexcore mesh for high-lift aircraft configuration," in *21st Annual CFD Symposium*, Bangalore, India, pp. 1–11, 2019.

[26] P. J. Richards, R. P. Hoxey, "Appropriate boundary conditions for computational wind engineering models using the k-ϵ turbulence model," *Journal of Wind Engineering and Industrial Aerodynamics*, vol. 46, pp. 145–153, 1993.

[27] P. J. Roache, "Quantification of uncertainty in computational fluid dynamics," *Annual Review of Fluid Mechanics*, vol. 29, no. 1, pp. 123–160, 1997.